Schweizerische Eidgenossenschaft
Confédération suisse
Confederazione Svizzera
Confederaziun svizra

Eidgenössisches Departement für
Umwelt, Verkehr, Energie und Kommunikation UVEK

Bundesamt für Energie BFE
Energieforschung

Schlussbericht

Analysis of induced microseismicity at the geothermal project Schlattingen (Canton Thurgau, Switzerland)

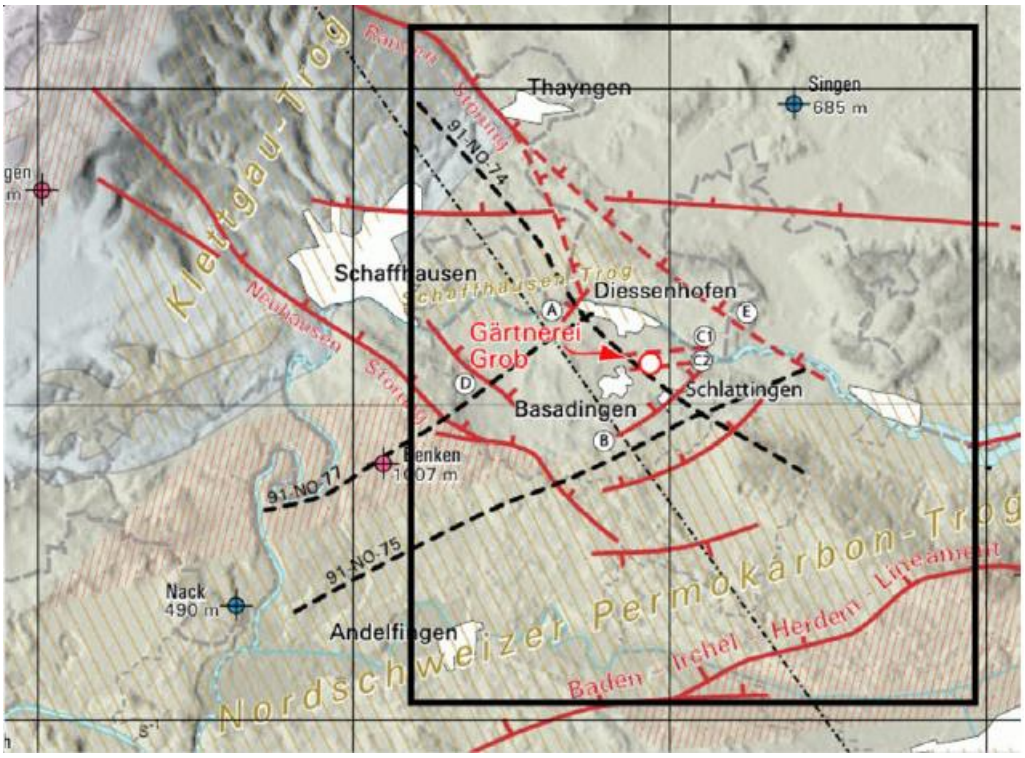

Datum: Dezember 2013

Ort: Bern

Das Projekt wurde durch die folgenden Organisationen Unterstützt:
Grob Gemüse- und Landbau
Im Bodenacker
8255 Schlattingen

Bundesamt für Energie BFE
Forschungsprogramm Geothermie
CH-3003 Bern
www.bfe.admin.ch
energieforschung@bfe.admin.ch

NAGRA
Hardstrasse 73
CH-5430 Wettingen
www.nagra.ch

Auftragnehmer/in:
Schweizerischer Erdbebendienst SED
Sonneggstrasse 5
CH-8092 Zürich
http://www.seismo.ethz.ch

Autor/in:
Toni Kraft, SED, toni@sed.ethz.ch
Marcus Herrmann, SED, marcus.herrmann@sed.ethz.ch
Tobias Diehl, SED, tobias.diehl@sed.ethz.ch

BFE-Bereichsleitung: Gunter Siddiqi, gunter.sidiqqi@adresse.ch
BFE-Programmleitung: Rudolf Minder, rudolf.minder@bluewin.ch
BFE-Vertragsnummer: SI/500864-01

nagra.

Project Report NPB 16-12

Analysis of induced microseismicity at the geothermal project Schlattingen (Canton Thurgau, Switzerland)

December 2016

T. Kraft, M. Herrmann & T. Diehl
Swiss Seismological Service at ETH Zurich

Restricted
Commercial in Confidence

National Cooperative
for the Disposal of
Radioactive Waste

Hardstrasse 73
P.O. Box 280
5430 Wettingen
Switzerland
Tel. +41 56 437 11 11

www.nagra.ch

nagra.

Project Report NPB 16-12

Analysis of induced microseismicity at the geothermal project Schlattingen, Thurgau

December 2016

T. Kraft, M. Herrmann & T. Diehl
Swiss Seismological Service at ETH Zurich

Restricted
Commercial in Confidence

KEYWORDS
Acid stimulation, seismic monitoring, induced seismicity

National Cooperative
for the Disposal of
Radioactive Waste

Hardstrasse 73
P.O. Box 280
5430 Wettingen
Switzerland
Tel. +41 56 437 11 11

www.nagra.ch

Table of Contents

List of Tables

List of Figures

1 Background and seismotectonic setting

1.1 Geothermal project Schlattingen

In 2007, Grob Gemüse und Landbau (Grob), a vegetable farmer in Schlattingen, Switzerland, initiated a deep geothermal project to reduce heating costs for their greenhouses. Based on a pre-study in 2007 and a feasibility study in 2010, the geothermal project for heat production was initiated and, after receiving a risk guarantee for the first borehole from Canton Thurgau, the project was initiated in November 2010.

A first vertical borehole (SLA-1) was drilled to a depth of 1'508 m bgl. into the crystalline basement (wellhead at 416.6 m asl.). The drilling started in December 2010 and was completed after several interruptions in January 2012. An intensive testing and well-logging program was performed in SLA-1 in 2012 (Frieg et al. 2015). Mini-frac testing at depth between 592 – 1'455 m bgl. indicate max. horizontal stress orientations around N6° and N161° and re-opening pressures range from 9.7 – 23.6 MPa (Klee 2012). After the testing program, the well was back-cemented to a level of 1'185 m bgl. The Upper-Muschelkalk aquifer (Trigonodus Dolomite; depth: 1'112 – 1'145 m bgl) was selected for chemical stimulation with deluded hydrochloric acid (HCl; 15 % – 20 %), which took place in three stages on October 21 and 24, 2011. Well head injection pressures reached 19 MPa. Due to frictional losses in the well, the down-hole pressure is believed to lie in the range of the re-opening pressure of the formation, at a maximum (Frieg et al. 2015). A long-term production test in April 2012 revealed that the stimulation increased the transmissivity in the aquifer by about one order of magnitude to $(1.33 – 4.65) \times 10^{-5}$ m^2/s, resulting in a flow rate of about 6 l/s. The aquifer temperature was evaluated to be about 62 °C (Frieg et al. 2015).

A second deviated borehole (SLA-2) was drilled in spring 2013 (February 14 – April 27). The well was driven into an eastern direction to reach higher temperatures predicted by thermo-hydraulic modelling (Frieg et al. 2015). This direction was also assumed optimal to penetrate the N-S striking, sub-vertical fracture sets documented in the first well and in local outcrops, and to reach a postulated zone of higher fracture intensity related to the Randen fault zone (Egil et al. 2014). A first unsuccessful well branch (SLA-2a) was abandoned and back-cemented, but the second branch (SLA-2b) successfully reached the Upper-Muschelkalk target horizon (Trigonodus Dolomite; depth: 1'113 – 1'174 m bgl), which was penetrated by the sub-horizontal well section over a length of 732 m (Fig. 2). Due to borehole stability issues the well was cased to 1'051 m MD before a geophysical logging program initiated.

The logging results confirmed that the borehole left the target formation for 49 m and penetrated the Lettenkohle in the hanging wall of the target formation. This short well section (1'818 – 1'867 m MD) was sealed off using a blank casing, after the logging. The logging also confirmed a predominantly NW-SE to NNW-SSE oriented fracture system in the Upper Muschelkalk. The deepest section of SLA-2 (1'950 – 2'013 m MD) has a high natural fracture density and contains NW-SE and N-S striking fractures with apertures of more than 1cm (Frieg et al. 2015). A major fault zone was found between 1'984 – 1'985 m MD containing three NNE-SSW-striking fractures with a cumulative aperture of 28 cm. During drilling, massive mud losses were observed in this section (April 24 – 30, 2013; up to 4'000 l/h and 70 m^3/d; Bläsi et al. 2014).

After completion and a short-term air-lift test (April 5, 2013), an acid stimulation in two stages was performed in the open-hole section of SLA-2 (i.e. two sub horizontal segments of the well in the Upper Muschelkalk target horizon (1'329 – 1'815 m MD and 1'868 – 2'013 m MD) completed with 5"-slotted liners) on May 6 and May 7, 2013. Well head injection pressures reached 30.2 MPa and injection rates were as high as 55.6 l/s. Most of the injected deluded

hydrochloric acid (HCl; 15 – 20 %) went into the already highly transmissive zone at the bottom of the borehole. A long-term pumping test between June 26 and October 13, 2013, revealed that the transmissivity and flowrate could not be increased significantly. After an evaluation and planning phase, a second acid stimulation was performed in SLA-2 in early 2015. For this stimulation the blank casing in the uppermost part of the target horizon was shot-perforated (February 17 – 19, 2015). An attempt to packer off the highly transmissive zone in the lower part of the well was not successful. The stimulation was performed in four stages on February 25 and February 27, 2015, again using deluded hydrocloridic acid (HCl; 15 %). Between March 4 and May 18, 2015, a long-term pumping test was performed in the stimulated well. The test results indicated that the transmissivity and flowrate could not be significantly increased.

The long-term pumping tests in both wells reviled that the groundwater of the Upper Muschelkalk aquifer contains considerable amounts of hydrogen sulfide (H_2S; up to 11 mg/l; Frieg (2015)). This gas caused some corrosion on the sensor cable of the seismometer installed in SLA-1 in 2013, of which more than 500 m had to be disposed of. During the pumping tests, H_2S also caused some odour trouble in the local communities.

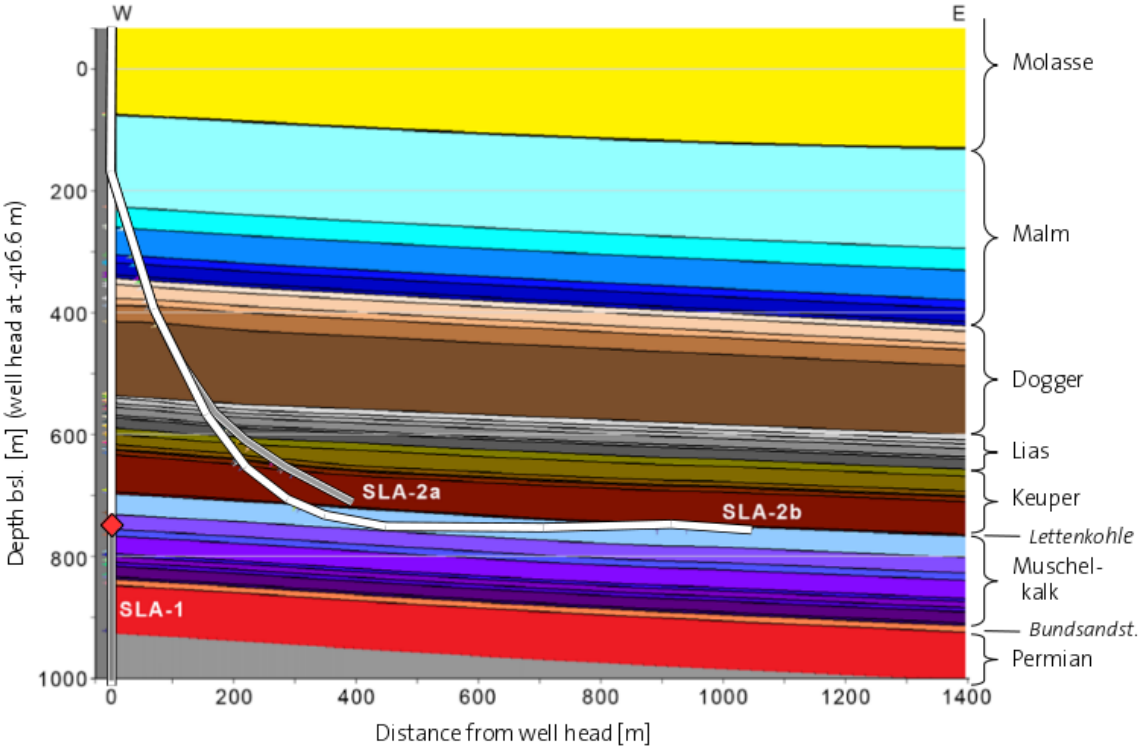

Fig. 1: Geological cross section indicating the projected trajectories of the geothermal wells SLA-1 (vertical) and SLA-2 (deviated towards east).

Geological units are indicated in color and labeled on the right. The location of the borehole sensor installed in SLA-1 in 2013 is indicated by a red diamond (modified after Blasi et al. 2014).

1.2 Geological setting

The geothermal site in Schlattingen is located 10 km east of Schaffhausen and 0.6 km south of the Rhine River close to the border to Germany. The drilling location is situated in the Swiss Molasse Basin between two regional normal faults. The Neuhausen Fault, about 5 km to the south is, well known from 3D-seismic surveys (Nagra 2000). The fault strikes NW and has a maximum offset of 100 m. The Randen Fault, some 2 km to the north, strikes approximately NW and has a maximum normal fault offset of 250 m (Nagra 2008). The Randen Fault is a well-exposed fault segment of the Freiburg-Bonndorf-Bodensee Fault Zone (FBBFZ; e.g. Paul 1948, Carlé 1955), a roughly 100 km long fault system, which runs approximately from the Kaiserstuhl in the Upper Rhein Graben across the Black Forest Massif to the Lake Constance. In the field, as well as in seismic sections the structure shows the characteristics of a normal fault but there are indications for a dextral transcurrent overprint. The Neuhausen and Randen Faults mark the westernmost bounding faults of the roughly NW–SE striking Hegau-Bodensee Graben, a crustal-scale structure associated with the volcanic fields of the Hegau region (Ibele 2015 and references therein). The main phase of extensional deformation in the Hegau-Bodensee Graben is reported to postdate Early Miocene times. Also the youngest preserved Molasse deposits are affected by normal faulting. Therefore, extensional to transtensional deformation in this area lasted until at least Late Miocene times and is probably still active today (Ibele 2015 and references therein). The tectonic process responsible for this deformation is not fully understood; some authors infer a kinematic relation with the seismically active Albstadt Shear Zone of Western Germany (e.g. Reicherter et al. 2008).

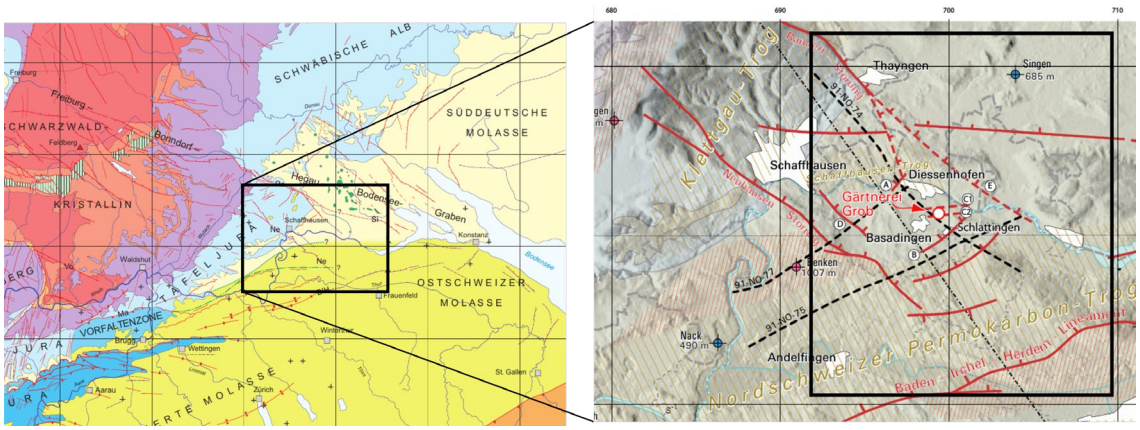

Fig. 2: Geological map of the wider surrounding of the study area.

The Schlattingen site is located at the northern rim of the Swiss Molasse Basin and at the SW corner of the Freiburg-Bonndorf-Hegau-Bodensee Graben between the well-documented Randen and Neuhausen Fault Zones. The NS-striking Albstadt Shear Zone is postulated to extend into the study area. The Hegau Volcanic Field marks the postulated intersection of these two crustal-scale fracture zones. Dominant basement structure is the Swiss Permo-Carboniferous Trough striking EW. The rectangle shown in the right map indicates the extend of the map in Fig. 3.

1.3 Natural seismicity

The natural seismicity in the closer vicinity of the Schlattingen geothermal project is indicated in Fig. 2. Before 1983 earthquake locations are largely uncertain due to the sparse network coverage at that time. The situation improved slowly after 1983. In both periods the seismicity is mainly confined to the areas north of the river Rhine and seems to follow the strike of the Hegau-Bodensee Graben. Earthquakes mainly locate to depths between 5 and 10 km in the basement and often occur in swarm-like sequences.

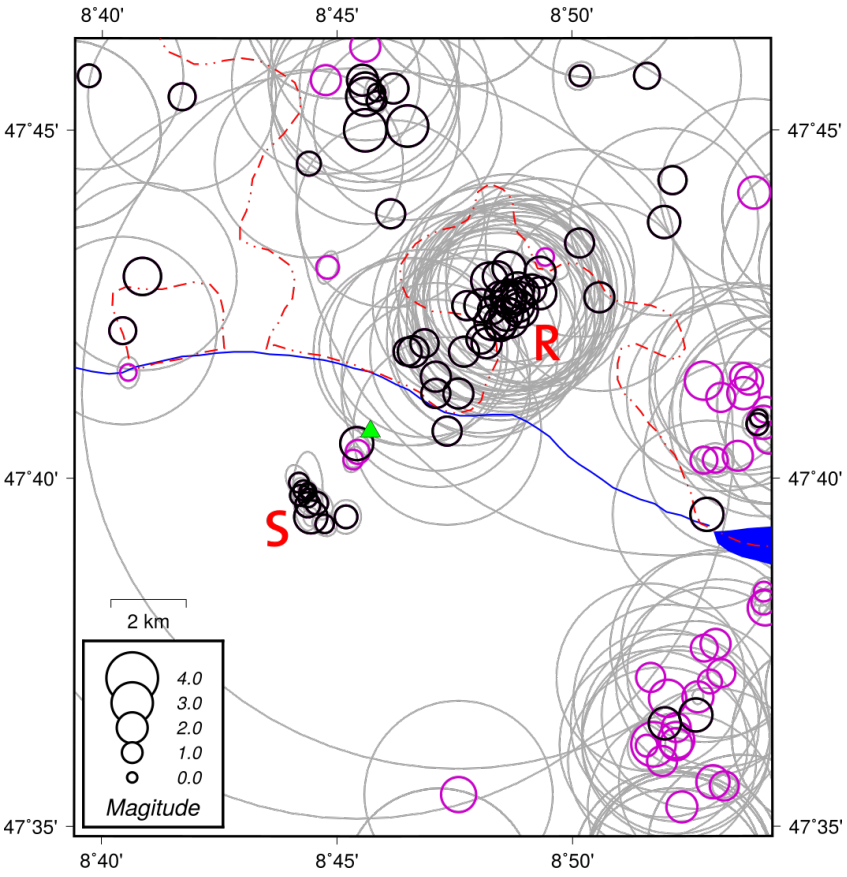

Fig. 3: Natural seismicity in the vicinity of the study area.

Earthquakes since 1983 are indicated by black circles, older earthquakes are shown as magenta circles. The location uncertainties is indicated by gray ellipses in both cases. Earthquakes sequences near Schlattingen (2015) and Ramsen (1983) are indicated by the red capital letters. The green triangle marks the location of the Schlattingen geothermal project.

In 1983 an earthquake swarm occurred between the communities Diessenhofen (D) und Ramsen (CH), about 5 km NE of the Schlattingen geothermal project. Within only 2 weeks, 40 earthquakes of magnitudes between ML1.2 and ML2.8 were located by the SED. The source depths of the events was reliably determined to about 8 km with the help of a 4-station seismic network installed in the area (Fig. 5). The seismological analysis revealed a dextral, NNW-SSE striking fault with steeply dipping fault plane. Similarly oriented structures also exist in Hegau in the near vicinity.

Between September 2014 and May 2016, the SED detected and located 9 earthquakes close to the town of Basadingen-Schlattingen about 2.5 km SW of the Schlattingen geothermal project, using routine methods. Seven of these events occurred between May and July 2015 with a maximum ML of 2.2 on May 31st. The routinely determined depths of these events range from 5 to 7 km. Due to the temporal and spatial vicinity of this sequence to the Schlattingen site, the swarm was to a large part recorded by the seismic monitoring network operated at the site (see below) and was analyzed in detail. Diehl et al. (2016) were able to identify and relocate a total of 21 events of this sequence. The high-precision relocations in combination with the focal mechanism of the ML2.2 event suggest a NE dipping normal fault in the crystalline basement. The structure imaged by microearthquakes might be related to the Neuhausen Fault, which is mapped as NE-dipping extensional feature in the Mesozoic Sediments (Nagra 2000). The sequence has been active irregularly since at least 2003 activity (Vouillamoz et al. 2016)

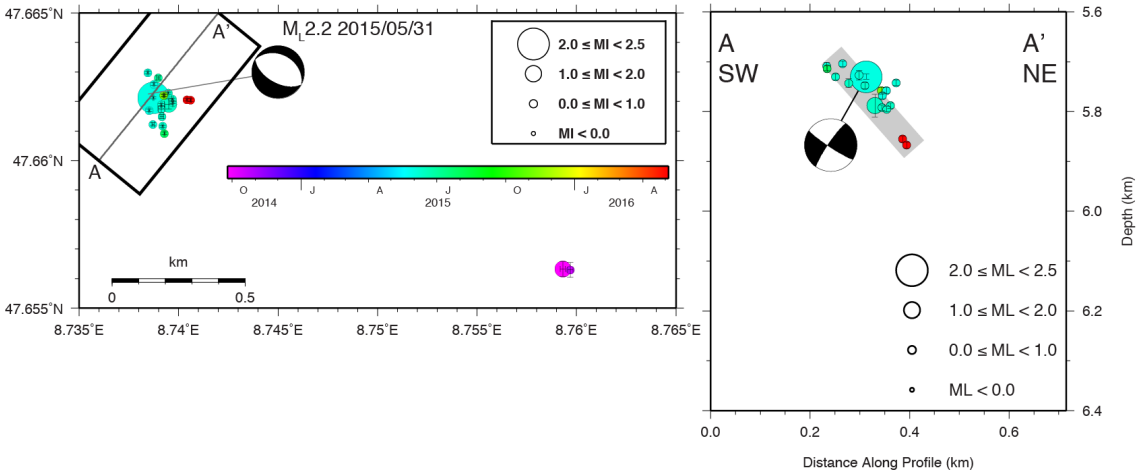

Fig. 4: Relative relocations of the Basadingen-Schlattingen sequence between September 2014 and May 2016 from Diehl et al. (2016).

Left: map view; Right: vertical cross-section along an SW-NE striking profile A-A'. Colors indicate origin time of the events. The focal mechanism of the ML 2.2 event of May 31st is indicated. Relocations in combination with the focal mechanism suggest a NE dipping normal fault in the crystalline basement.

The known focal mechanisms of natural earthquakes in the larger vicinity of the Schlattingen geothermal project locate in the basement and are consistent with shortening directed in NNW direction (Kastrup et al. 2004). However, compared with active tectonic regions, the seismicity is low and GPS-derived strain rates in the Molasse Basin of north-eastern Switzerland are well below 0.5 mm/y (Sue et al. 2007).

2 Induced seismicity at the Schlattingen project

2.1 Monitoring network

The Schlattingen Geothermal project was monitored by the Swiss Seismological Service in the framework of the GEOBEST project, which was funded by the Swiss Federal Office of Energy (BFE). The monitoring started in June 2013 and was performed in three operation phases (Fig. 5), which were aligned with hydraulic operations at the geothermal well SLA-2 (Acid-stimulations) or the occurrence of natural seismicity.

Due to extra funding from BFE, the SED was able to procure a borehole sensor and 3 km cable that had been formally used in the geothermal project in Basel. Thankfully, the project owner Grob allowed the SED to install the borehole sensor at the bottom of the back-cemented well SLA-1 (Fig 1). The sensor was installed during the drilling phase of the horizontal well SLA-2 by Geo Explorers Ltd. using a cable winch of Kabelwerke Brugg. The installation was quite complex as the truck of the drill rig was blocking the rig cellar of SLA-1, and access to the well was only possible after removing one of the truck's wheels. After the sensor was slowly lowered to the target depth, the signal was recorded using a RefTec 130 24-bit digitizer with 1000 Hz sampling rate. For the first weeks the station was operated on battery, but later power was provided from an on-site generator of the drilling company. Unfortunately this introduced strong 50Hz electronic noise that could not be improved. The borehole sensor was operated only in the first operation phase between April 17 and June 26, 2013 and had to be removed for the long-term pumping test after that. Unfortunately, the lowest 500 meters of the sensor cable were heavily corroded by H_2S gas. The outer armor of the cable began to break when the damaged part of the cable was passing over the deflection pulley, but the instrument could safely be recovered from the well.

The borehole station QSLA0, described above, build the central part of the seismic monitoring network, which was completed by four surface stations. One station was located close to the well heads of SLA-1 and SLA-2, near the Grob greenhouses (QSLA2). This station actually consisted of two mobile stations: one strong-motion and one conventional weak-motion station. The former was installed for the unlikely case that a stronger earthquake would be induced by the operation in SLA-2, which could cause the weak motion instruments to clip. The latter represented the central station of a microseismic surface network with three further stations distributed at equal-angle distances on a 2.5 km-circle centered on the Schlattingen wells. The chosen network geometry is known as the triangular quadripartite network, and is known to be the optimal network for location earthquake at a depths of half the outer-station-circle radius below the center of the network (Rabinowitz & Steinberg 1990). The network geometry was rotated in such a way that all outer-circle stations were located in areas with relatively low seismic noise. All surface stations where operated on batteries and were visited every 2 – 3 weeks for data download and battery exchange. Data gaps occurred on all stations due to battery outage or hard disk failure. Fortunately, at least one station was always operational when others failed and no gap in overall monitoring occurred.

The data recorded at the seismic stations was manually downloaded to the SED data archive, where it is stored on redundant hard disks in standard seismic formats for waveform data and instrument metadata. This ensures the long-term availability and usability of the data for the scientific community. The data can be made available via the SED data access portal (http://arclink.ethz.ch) to closed user groups or as open-access data.

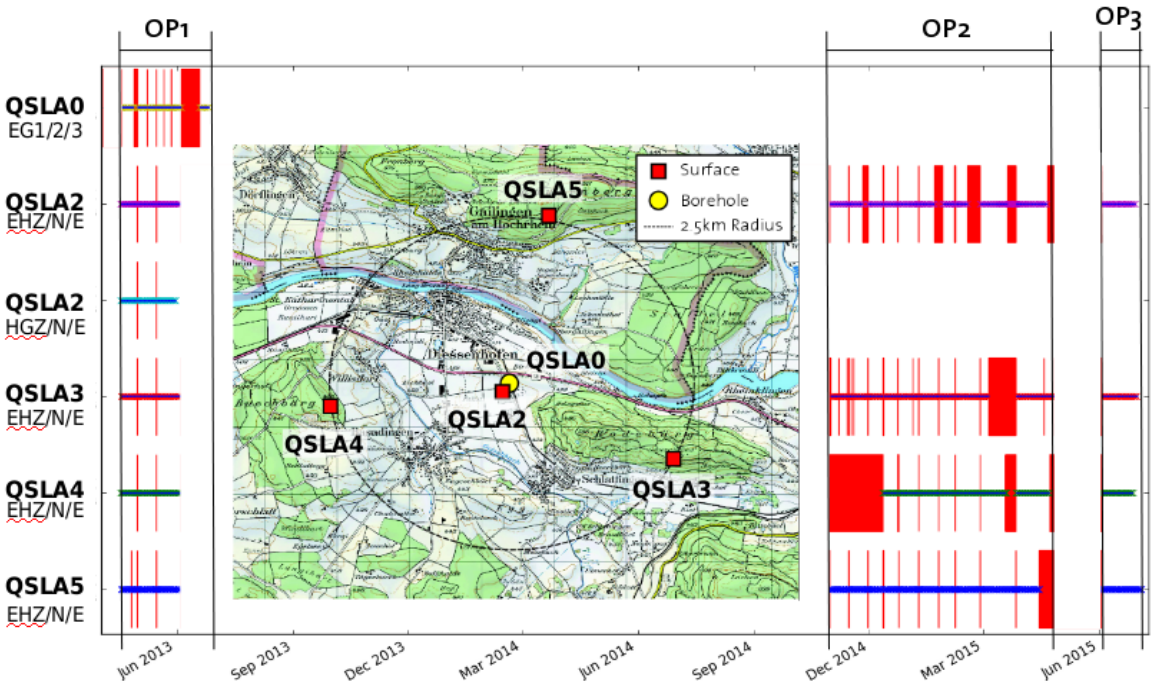

Fig. 5: Geometry and operation periods of the seismic monitoring network at the Schlattingen geothermal project.

Map indicates stations geometry and station type. Timeline indicates on-time of individual station by colored horizontal line. Data gaps are indicated by red bars. The three operation periods are indicated by vertical black lines. Station and channel names are indicated on the left.

2.2 Data analysis

As the seismic network was operated in off-line mode, the data could not be included in the routine data processing of the SED. Event detection was, therefore, done using different stand-alone tools. We decided to use a combination of energy-based detection algorithm (STA-LTA; e.g. Allen 1978) and manual inspection of continuous waveforms. Both methods were applied to the borehole station QSLA0 for its total operation period. In both cases, the data was high-pass filtered using a 90Hz high-pass of 6th order. The detected events were analyzed for waveform similarity in a hierarchical cluster analysis. In this way, 25 microearthquakes families where identified and the strongest event of each family selected as a template event for the subsequent analysis steps.

The 25 template events where feed into the newly developed template matching software of the SED (Herrmann et al. 2017). In this algorithm, the continuous data of the station with the highest signal-to-noise-ratio (snr) for the earthquake sequence of interest is scanned using a cross-correlation technique using a seismogram template set from the same station. The template matching technique is successfully being applied since several decades in many fields of science and engineering, and is known to be highly sensitive even below the station's noise level (Gibbons & Ringdal 2006, Shelly et al. 2007).

To compensate for the limited temporal coverage of station QSLA0, the template matching scan was extended to two further stations. We used the second best station in terms of snr, QSLA3, to scan the operation periods for which the borehole station was not operational with the highest possible sensitivity. Further we scanned the SED station with the best snr for the induced

sequence, TRULL, to cover the total lifetime of the Schlattingen project (December 2010 – July 2017 (end of analysis for this report)). For each scan the templates events were chosen from the same 25-template set of station QSLA0. Yet, the number of templates had to be reduced at station QSLA3 (6) and station TRULL (2) due to their insufficient snr at stations at larger distances.

The three template matching detection lists from stations QSLA0, QSLA3 and TRULL were combined to a single list. The combined list contains 399 detections between Apr 24, 2013 and February 27, 2015. The largest event detected had a magnitude of ML0.4 and occurred on February 25, 2015, at 18:24:35.3 (utc) as part of the second stage of the first acid job in 2015. The event was too small for the study area to be detected by the automatic monitoring system of the SED. After the detection with the procedure described above, the event was manually located and its magnitude determined following the SED standard rules. This magnitude was used as a reference point to derive the magnitudes of the smaller events, as described in the following.

First, the magnitudes of the detections at station QSLA3, ML_{corr}, were estimated using a linear relationship of the form $ML_{corr} = \log(A) + A_0$, where A is the 3-component root-mean-square amplitude of the detection at QSLA3 and A_0 is a calibration constant that assures that the magnitude of the reference event (the ML0.4 mentioned above) is $ML_{corr} = 0.4$. Using this magnitude approximation for a specific earthquake family and station combination is valid if the magnitude is smaller than approximately ML2.0 in Switzerland. The seismic waves of these events have lost most of the high frequency content due to seismic attenuation when reaching the stations. This low-pass filtering removes the magnitude dependency of the frequency content of the seismograms of these events, and they become amplitude-scaled copies of each other if they are located close enough. This effect was recently described and explained in more detail by Deichmann (2017).

The same approach as for QSLA3 was used to approximate the magnitudes for the detections at station TRULL.

A slightly different approach had to be used to approximate the magnitudes of the detections at the deep borehole station QSLA0. Due to the close distance of the sensor to the earthquakes (0.7 – 1.5 km), small differences in source location and radiation patterns have a strong influence on the amplitude scaling. We, therefore, derived individual magnitude approximation relations for each of the 25 template families using ML_{corr}(QSLA3) as reference magnitude (Fig. 6). As the detections are assigned to these families based on waveform similarity, the before mentioned effect should be minimized.

Comparing the three ML_{corr} stations magnitudes for events detected at all three stations, shows a very good agreement with only a small scatter of +-0.1 magnitude unit. In the final catalog the median was used for detections with more than one ML_{corr} station magnitude.

All induced earthquakes detected in this study that could be associated with activities at the geothermal project Schlattingen had magnitudes equal or smaller ML0.4. Earthquakes of this size can only be detected by seismological instruments and are in the following for simplicity referred to as microearthquakes even though more detailed classifications have been proposed (Bohnhoff et al. 2010).

72 of the detected microearthquakes were strong enough to be located with the routine analysis software of the SED, SeisComp3. Locations were calculated using the 3D velocity model of Husen et al. (2003) and a fully probabilistic inversion approach (Lomax et al. 2001).

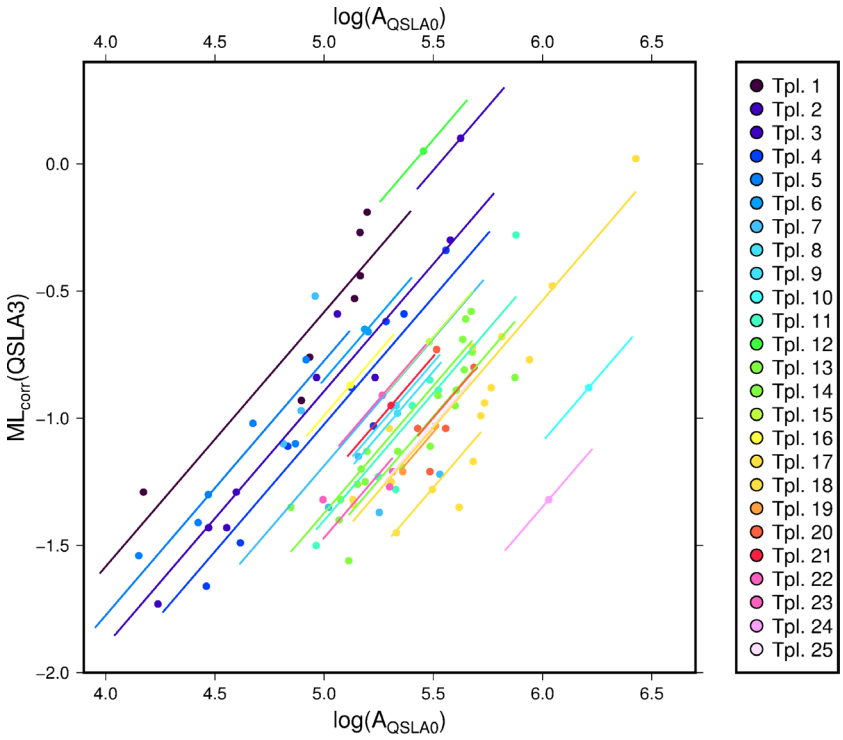

Fig. 6: Magnitude regression analysis for 25 template families detected at QSLA0.

A linear regressions (colored lines) between $\log(A_{QSLA0})$ and ML_{corr}(QSLA3) performed for the 25 template families identified at station QSLA0, where A_{QSLA0} is the 3-component root-mean-square amplitude of the detection at QSLA0. The slope of the regression was fixed to 1. Dots indicate all detections at QSLA0 with available ML_{corr}(QSLA3). Colors indicate the association to the template families.

2.3 Results

The final earthquake catalog combines the detections found by template matching at the three stations QSLA0, QSAL3 and TRULL. The catalog contains 399 microearthquakes between April 24, 2013 and February 27, 2015, with magnitudes between ML_{corr}0.4 and ML_{corr}-2.6 (Fig. 7, 8, 9). These events are shown in Fig. 7, where the colors indicate if an earthquake was detected only at QSLA0 (red), only at QSLA0 and QSLA3 (yellow), or at all three scanned stations, including TRULL (blue).

Fig. 7 shows the largely different detection sensitivities of the three stations. Detection on station TRULL are only complete above a magnitude threshold of about ML_{corr}0.0. For periods in which only TRULL is available for scanning, earthquakes below this threshold will most likely not be detected. On the other hand, earthquakes with magnitudes larger than this threshold and with similar enough seismograms to the known template earthquakes – i.e. close enough to these events – would have been detected with a large certainty. Station TRULL was scanned from Dec 2010 to August 2016, but no earthquakes were detected outside of the operation periods of the QSLA-stations. This indicates that the operations at the Schlattingen geothermal site did not cause seismicity above magnitude ML_{corr}0.0 in the non-QSLA periods.

We further learn from Fig. 7, that station QSLA3 has a detection completeness of about ML_{corr}-1.0. The further below this threshold, the larger the probability that an earthquake is only

detected on station QSLA0. From this we can conclude, that in operation period OP2 and OP3 (Fig. 5), in which QSLA0 was not operating, no earthquake above ML_{corr}-1.0 at the Schlattingen site is missing in our detection catalog. As expected the detection sensitivity was highest when the borehole station was in operation in operation period OP1 (Fig. 5). The statistical analysis of the microearthquakes detected at station QSLA0 indicates, that the detection completeness was about ML_{corr}-1.9 in this period. The fact, that earthquakes down to ML_{corr}-2.6 were detected, highlights that the detection probability does not drop to zero below the completeness threshold immediately.

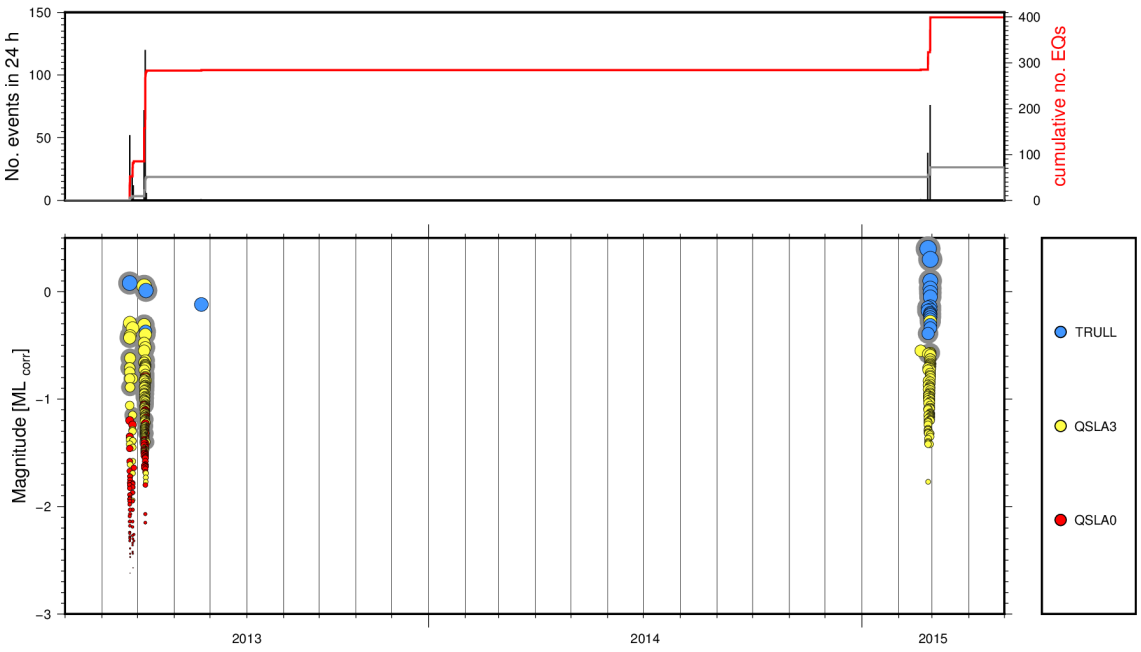

Fig. 7: Timeline of all 399 detected earthquakes in the scan period March 2013 – May 2016.

Detections from station QSLA0, QSLA3 and TRULL are combined to one catalog. Bottom: Dots indicate the detections and the color denotes the least sensitive station. Earthquakes detected on more than one station are shown with the median station magnitude. Dots with gray outlines represent located earthquakes. Top: Cumulative number of detected (red) and located (gray) earthquakes. Histogram of detected events in 24 h (black).

Fig. 7 illustrates, that the large majority of the detected earthquakes occurred in short seismic sequences that lasted from a few hours to a few days lengths. The sequences occurred between Apr 24 and May 8, 2013, and between Feb 19 and Feb 27, 2015, and are illustrated in Fig. 8 and 9, respectively. The sequences can all be associated with operations at the well SLA-2:

- First microearthquakes were detected on April 24, 2013 around 10:06 UTC. Until 14:07 UTC, 37 events with magnitudes between ML_{corr}0.1 and ML_{corr}-2.3 were detected. At around 16:49 UTC a second burst of 15 events with magnitudes between ML_{corr}-0.4 and ML_{corr}-2.6 started and lasted until 18:18 UTC. A third burst of 30 microearthquakes occurred between 20:28 on April 26 and 05:45 on April 27, 2013 with magnitudes between ML_{corr}-0.3 and ML_{corr}-2.6. The episode ended with three tiny microearthquakes (MLcorr>-1.6) around 21:31 UTC on the same day.

  All of these seismicity bursts fall into the period of massive mud losses that occurred between April 24 and April 30, 2013, during the construction of SLA-2. At that time, the drilling penetrated a major fault zone between 1'984 – 1'985 m MD containing three NNE-SSW-striking fractures with a cumulative aperture of 28 cm. The mud losses reached 4'000 l/h and 70'000 l/d (Bläsi et al. 2014). The observed seismicity was most likely caused by the hydraulic reactivation of parts of this fracture zone by the mud. This reactivation occurred as consequence of small overpressures caused by higher mud weights that were required to deal with borehole instabilities in the inclined borehole section (dP ~ 1.3-1.8 MPa: mud weight: 1.11 – 1.15 kg/l; depth: ca. 1'175m TVD). This is an indication that the fractures are nearly optimally orientated for reactivation in the present tectonic stress field.

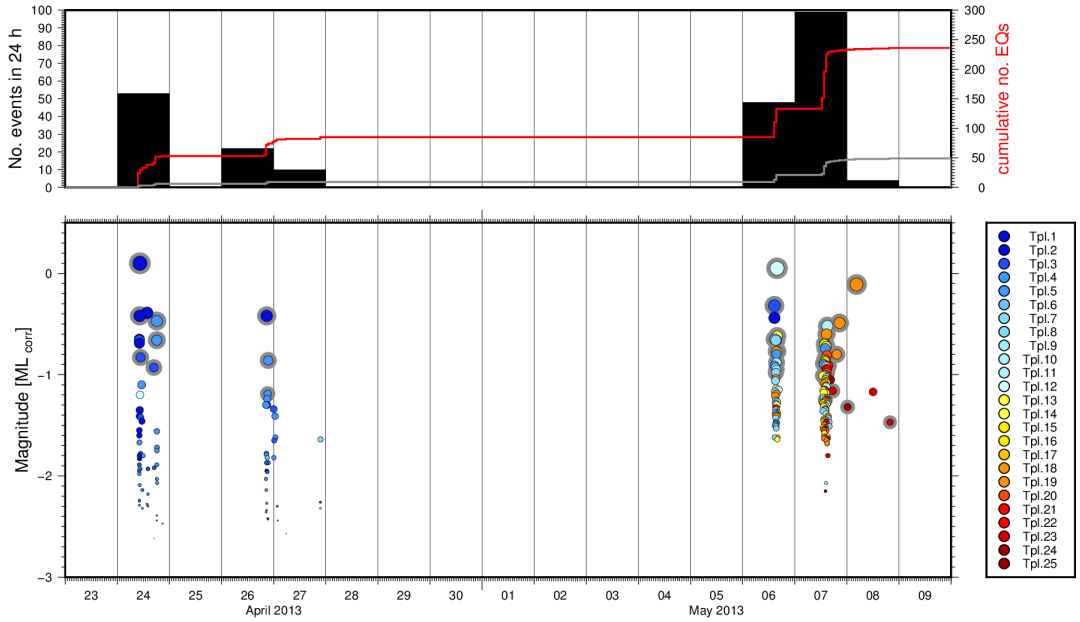

Fig. 8: Timeline of the 284 earthquakes detected at station QSAL0 (borehole) between April 23 and May 10, 2013.

Detections from station QSLA0. Bottom: Colored dots indicate detected earthquakes. Colors indicate association of the detections to one of 25 template used for scanning. Dots with gray outlines represent located earthquakes. Top: Cumulative number of detected (red) and located (gray) earthquakes. Histogram of detected events in 24 h (black).

- Two further seismicity burst were detected on May 6 and May 7, 2013. The first one started at 14:38 UTC and lasted until 16:29 UTC and consisted of 72 microearthquakes with magnitudes between ML_{corr}0.1 and ML_{corr}-1.6. The second burst, with 113 events, set in at 12:56 UTC and lasted until about 15:23 UTC. The magnitudes ranged between ML_{corr}-0.4 and ML_{corr}-2.2. The second burst was followed by 13 events with inter-event times up to several hours, and magnitudes between ML_{corr}0.0 and ML_{corr}-1.7. The last of these 13 events was detected on May 8 at 19:53 UTC.

  The two seismicity bursts on May 6 and May 7, 2013, are clearly related to the first and second stage of the first acid stimulation in SLA-2. The first stage started injection on May 6 at 14:35 UTC; pumps were stopped at 15:46 UTC. Wellhead pressure stayed above hydrostatic for a longer period after shut-in; when the hydrostatic level was reached is not documented in the field logs. A total volume of 331 m^3 of water and deluded hydrochloric acid (HCl; 15 % – 20 %) was injected with well head pressures up to 30.2 MPa and flow rates of up to 3.26 m^3/min. The largest event (ML_{corr}0.1) occurred at 15:50 UTC, four minutes after shut-in.

  The second stage started injection on May 7 at 12:32 UTC and pumps where stopped at 14:49 UTC. Again, wellhead pressure stayed above hydrostatic for a longer period after shut-in; when the hydrostatic level was reached is not documented in the field logs. A total volume of 390 m^3 of water and deluded hydrochloric acid (HCl; 15 %) were injected with well head pressures up to 25.2 MPa and flow rates of up to 3.35 m^3/min. The largest event (occurred ML_{corr}0.0) occurred at May 8 at 04:25, 13.6 hours after shut-in.

  In both cases, the strong temporal correlation between the onset of the seismicity and the initiation of the hydro-chemical stimulation indicates a causal relationship. First statistical analyses of the induced earthquakes in May 2013 indicate a magnitude-frequency distribution with a high b-values (Kraft et al. 2017). High b-values are also reported from induced earthquakes in hydraulic fracturing (e.g. Davis et al. 2013), which could indicate, that this was also the dominant stimulation style here. A mode-I fracture opening during stimulation and insufficient self-propping after pressure relieve might also explain the limited success of the acid stimulation reported by Frieg et al. (2015).

- An isolated earthquake with ML_{corr}-0.1 was detected on June 23, 2013 at 18:31 UTC, 46 days after the last microearthquake directly following the acid stimulations. The event is associated with template 25 of station QSLA0 and should, therefore, be located close to the other events of the first acid stimulation. The event could not be located because the QSLA surface network had already been dismantled at that time.

  So far, the event could not be associated with any activity at the wells SLA-1 or SLA-2. It might just be a late aftershock of the seismicity induced by the first acid stimulation. Due to the waveform similarity of the event with microeartquakes associated with the first acid stimulation a natural origin seems less likely.

- After long seismic quiescence of nearly 1.7 years, a single seismic event with ML_{corr}-0.6 was detected on February 19, 2015, at 13:13 UTC.

  The events fall into the period when perforation shots were fired in SLA-2 to re-open the casing for the second acid stimulation. The event was too small to be located, but its association to template 6 of station QSLA3, which indicates: It's rather a micoearthquake located close to this template family, than a direct recording of a perforation shot.

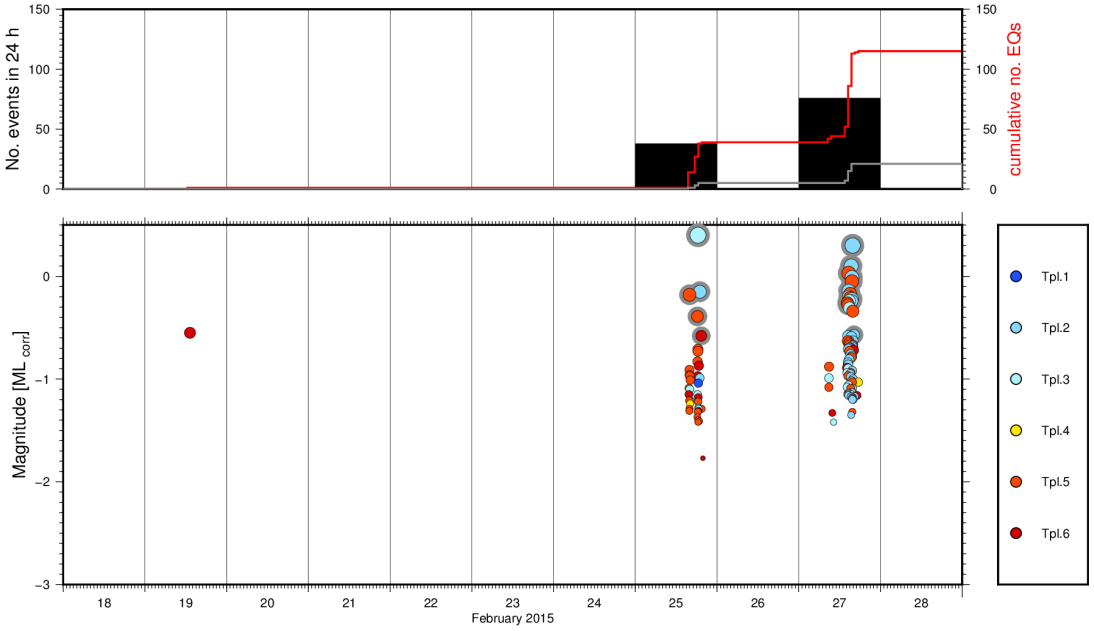

Fig. 9: Timeline of 115 earthquakes detected at station QSAL3 between February 18 and 28, 2015.

Detections from station QSLA3. Bottom: Colored dots indicate detected earthquakes, time axis is in UTC. Colors indicate association of the detections to one of 6 template used for scanning. Dots with gray outlines represent located earthquakes. Top: Cumulative number of detected (red) and located (gray) earthquakes. Histogram of detected events in 24 h (black).

- Two further bursts of seismicity were detected on February 25 and February 27, 2015. Taking a closer look reveals that each of this bursts can be further divided into at least two sub-bursts. The resulting four sub-bursts in the seismicity have the following properties. The first sub-burst consists of 13 events with magnitudes between ML_{corr}-0.2 and ML_{corr}-1.3 that occurred between 15:45 and 16:12 UTC on February 25. The second sub-burst consist of 25 earthquakes with magnitudes between ML_{corr}0.4 and ML_{corr}-1.8 that occurred between 18:16 and 19:52 UTC on February 25. The third sub-burst contains only 5 tiny earthquakes with magnitudes between ML_{corr}-0.9 and ML_{corr}-1.4 and lasted that occurred between 08:51 and 10:30 UTC an February 27. The last sub-burst has 71 earthquakes of magnitudes between ML_{corr}0.3 and ML_{corr}-1.4 and lasted from 14:11 to 17:31 UTC on February 27.

  It is highly probable, that the four sub-bursts are associated with the second acid stimulation of SLA-2, which took place on February 25 and 27, 2015, and consisted of four injection stages. Unfortunately, only a graphical documentation of the first and fourth stage of this acid job (Frieg, 2015) was available to us at the time of writing this report, and an unambiguous correlation between the seismicity and the injection activities could not be established. This is mainly due to the lack of knowledge on what time standard was used in the injection parameter plots.

  Assuming the plots were in UTC, the first stage on February 25 could be summarized as follows. Injection test from 15:46 to 16:01 UTC; wellhead pressure reached 15 MPa and flow rates 3.0 m^3/min, with an injected volume of about 30 m^3. Acid stimulation from 16:29 to 17:03; wellhead pressure reached 20 MPa and flow rates 3.5 m^3/min with an injected volume of (water and 15 % HCl) of 120 m^3. This timeline would indicate, that the

seismicity of sub-burst one would have been induced by the injection test and that no seismicity was associated with the acid stimulation in the first stage of the second acid stimulation.

The largest earthquake detected in this study ($ML_{corr}0.4$) occurred on February 25 at 18:24. We can only speculate that this event is correlated with the second stage of the acid job on this day. The injection parameters to solve this questions were not available at the time of writing.

Still assuming UTC timing, the fourth stage on February 27 can be summarized as follows. Acid stimulation from 14:35 to 17:01 UTC; wellhead pressure reached 20 MPa and flow rates 3.5 m^3/min, with an injected volume of (water and 15 % HCl) of 396 m^3. This would indicate that the fourth sub-burst in seismicity coincided with a large part of the fourths stage of the second acid stimulation. Yet it seems that seismicity has started already 20 min before the stimulation. If this early start could be explained by some other activity at the well could not be answered with the information available to us at the time of writing.

The second largest earthquake ($ML_{corr}0.3$) detected in this study occurred on February 27 at 15:49. The injection parameter plots of Frieg (2015) suggest that the event occurred during the fourth stage of the second acid stimulation, at a wellhead pressure of about 15 MPa and an injection rate of about 2.6 m^3/min. At the time of the event about 225 m^3 of fluids (water and 15 % HCl) had been injected.

The 72 located microearthquakes are shown with their location uncertainties in Fig. 10. The figure shows the single event locations that were determined using a slightly modified form of SED routine analysis. Due to the small magnitudes of the events analyzed in this study, and due to the non-standard deep borehole station QSLA0, waveform filters for onset-time determination had to be adapted. The resulting uncertainties for single event location were in the order of 1 km and slightly below. The largest uncertainty was observed in the depth coordinate of the earthquakes.

All located microearthquakes detected by the template matching analysis on station QSLA0, QSLA3, and TRULL locate east of the wellheads of the Schlattingen boreholes. The centroid of the seismic cloud located on the trajectory of the borehole SLA-2 about halves way between its wellhead and landing point. All of the events have source depths of about 1 km (bsl.). Considering the depth uncertainty (around +- 1 km) the source depths must be considered unconstrained, yet restricted to the upper most two kilometers.

The seismic cloud of the 2013 events seem elongated along the trajectory of SLA-2, whereas the seismic cloud of the 2015 seismicity appears to be elongated in the NNW-SSE direction. The dimension of the seismic cloud seems to extend to around 1.5 km in the N-S direction and slightly less than 1 km in the E-W direction. Due to the uncertainties of the singe event locations (around +- 1 km), the geometry of the seismic cloud cannot be confirmed with much confidence.

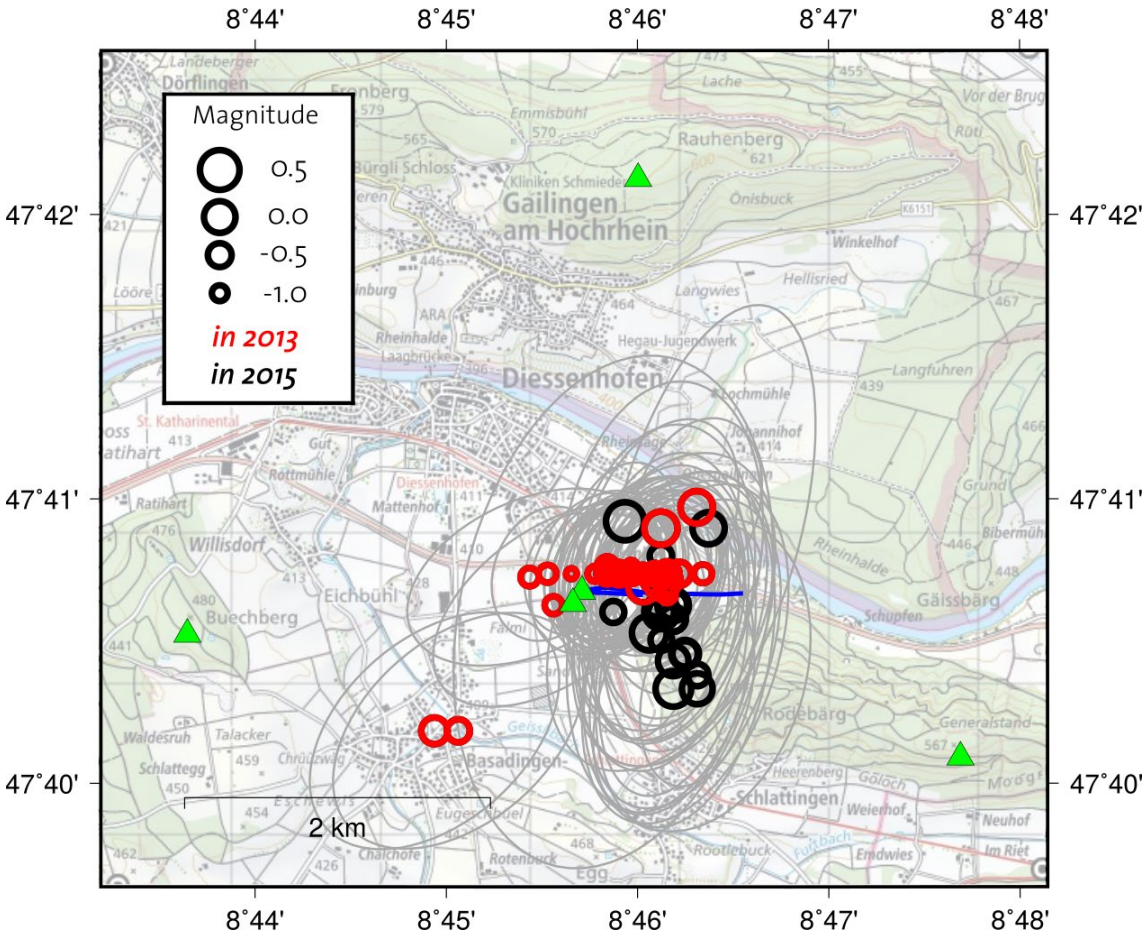

Fig. 10: Epicenter map of 72 microearthquakes located in this study.

Black and red circles indicate earthquake epicenters in 2015 and 2013, respectively; gray ellipses show their uncertainties; green triangles indicate the Stations of the QSLA network. The trajectory of borehole SLA-2 is indicated in blue. Background map from swisstopo. Two events at some distance in the SW of the wellhead belong to the natural earthquake sequence described in section 1.3, that has been active irregularly since at least 2003 activity (Vouillamoz et al. 2016).

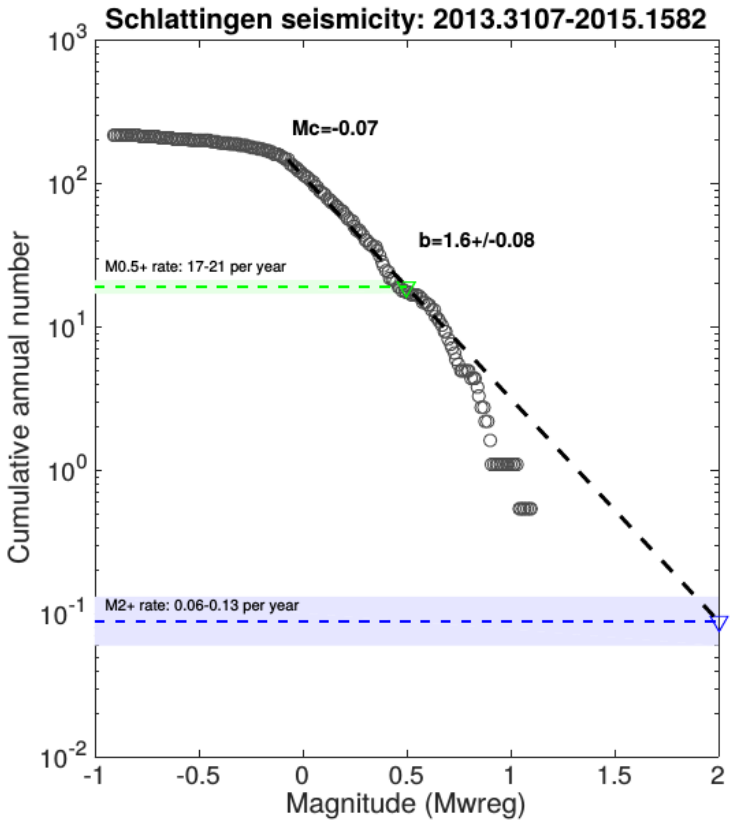

Fig. 11: Frequency magnitude distribution of the 399 detected microearthquakes.

Magnitudes were converted to moment magnitude, Mw, using the relation of Edwards et al. (2015). Estimated occurrence rate of Mw1 (ML0.3) and Mw2 (ML1.7) earthquakes are indicated in green and blue, respectively. Overall detection completeness, Mc, is Mw-0.1 (ML-1.3).

First results of a relocation analysis (Kraft et al. 2017), using high-precision cross-correlation techniques indicate: 1) that seismicity is falling on a NNW-SSE oriented structure; 2) that seismic events seem to occur at distances of several hundred meters away from the borehole trajectory of SLA-2. This result could indicate that a preexisting fracture zone was reactivated by the fluid injection and mud losses at the SLA-2 well. Fracture systems of this orientation have been identified by well logging in both Schlattingen boreholes (see Frieg et al. 2015, and references therein), and dominate the fracture sets mapped in surface outcrops in the region (Egli et al. 2014, Madritsch 2015).

The magnitude frequency distribution (FMD) of the 399 microearthquakes detected by template matching is shown in Fig. 11. For the calculation of the FMD, magnitudes were converted to moment magnitude, Mw, which is common practice for seismic hazard analyses. For the conversion we used the relationship of Edwards et al. (2015) derived for the induced sequences in Basel and St. Gallen. We find an overall b-value of $b = 1.6$, which is relatively high compared to b-values observed for tectonic earthquakes, which are in the order of b=1. High b-values are usually observed in fluid driven earthquake sequences. Our b-value would, therefore, fit the scenario of an injection induced seismic sequence described here. The FMD shows deviation from a purely linear behavior in the magnitude range above Mw. This deviation can to some part be explained by the short temporal duration of the seismic burst that causes a characteristic roll-off in the FMD. The other non-linearity might be related to non-stationary

behavior of FMD in different parts of the timeline of the seismic sequence. First results of a more detailed analysis indicate that this is the case (Kraft et al. 2017).

The FMD of the 399 earthquakes indicates an overall detection completeness of Mw-0.1 (ML-1.3). Obviously, the detection sensitivity changed due to the changing network density over the analyzed period. More detailed estimates of the detection sensitivity in specific periods were discussed above.

By fitting and extrapolating the linear part of the FMD in Fig. 11, we can derive expected occurrence rates for larger events. The values given in the Fig. 10 are normalized to annual occurrence rates. Due to the short duration of the seismic bursts observed in this study it makes however more sense to refer to daily rates. Doing this we estimate an occurrence rate of (5 – 6) 10^{-2} for earthquakes equal or larger Mw1.0 (ML0.3), and occurrence rates of (1.6 – 3.6) 10^{-4} per day for earthquakes equal or larger Mw2.0 (ML1.7). Considering that two earthquakes with magnitudes equal or larger Mw1.0 (ML_{corr}0.3) were detected in seven days of seismic activity in this study, the occurrence rate seems to be slightly underestimated at least for this magnitude range. A more detailed statistical analysis of the seismic bursts observed in this study is underway and may find an explanation for the underestimation.

3 Conclusions

The natural seismicity in the vicinity of the Schlattingen geothermal project is low. The known earthquakes occurred in the crystalline basement at depths between 5 – 10 km and seem to be associated with the Neuhausen and Randen faults, which are part the crustal scale Freiburg-Bonndorf-Bodensee Fault Zone. The small number of earthquake focal mechanisms available for the area have strike-slip to normal-faulting character and seems to be a consequence of the superposition of the NNW-SSE shortening of the Alpine foreland and the extension in the vicinity of the Hegau-Bodensee Graben (Madritsch 2015).

Despite the low natural background seismicity, the Schlattingen project has experienced the occurrence of an earthquake sequence with maximum magnitudes up to ML2.2 in its short lifetime. Due to the local seismic network, installed for the monitoring of the project, it was possible to constrain the location and depth of this sequence with high confidence and to rule out a causal relationship with the geothermal project. Without the local network, the location uncertainties – especially the in depth – would have been too large to exclude this relationship. This highlights the importance of local seismic monitoring for the discrimination of natural and induced seismicity in the vicinity of a geotechnical project.

We analyzed the seismicity in the period between December 2010 and August 2017 using a highly-sensitive template matching detection technique on. The scan is complete above ML0.0 and detected only seven earthquakes (Tab. 1). All of these earthquakes can be associated with operations in borehole SLA-2 (Tab. 1), of the Schlattingen geothermal project. During the operation periods of the local network, the sensitivity of the detection could be improved dramatically, and a total of 399 microearthquakes between ML0.4 and ML-2.6 were found. All these 399 events - which including the seven earthquakes above ML0.0 (Tab. 1) - are confined to short seismic bursts in April and May 2013, as well as in February 2015. Again, all microearthquakes are closely linked to operations in borehole SLA-2.

The uncertainty in the magnitudes given in this report is large in an absolute sense, i.e. we expect that a constant bias exists with respect to the true magnitude of the earthquake. The SED often overestimates the magnitudes of earthquakes below ML1.0, as the magnitude formula used is not calibrated for station distances smaller than 20 km (Edwards et al., 2015). The standard procedure of SED is, therefore, to exclude stations within this uncalibrated distance range from magnitude estimation. For very small earthquakes this procedure must often be violated and station magnitudes from the uncalibrated distance range, which are usually overestimated, have to be used for magnitude estimation. As a consequence, the resulting earthquake magnitude may be overestimated too.

The magnitudes of the induced Schalttingen seismicity are consistent in a relative sense, i.e. with respect to one another. The absolute values were calibrated to the largest earthquake observed in this study with an SED magnitude of ML0.4. In the light of the discussion above, this magnitude must be considered an upper bound and the real magnitude of the earthquake – and, therefore, of all 399 events analyzed in this study - might be up to 0.5 magnitude values smaller than estimated.

Tab. 1: List of induced Schlattingen earthquakes with magnitudes $ML_{cor\ r} \geq 0.0$.

The locations and uncertainties for the routine analysis are given in absolute coordinates. The oeration the event is associated with is indicated in tha last column: acid <job>/<stage> or mud loss.

Source time	**Coordinate**			**Uncertainty**		**Magnit.**	**Operation**
UTC	Latitude	Longitude	Depth	Horiz.	Depth	ML_{corr}	In SLA-2
2015-02-25 18:24:34	47.68202	8.76558	2.1	0.8	0.8	0.40	acid 2/2
2015-02-27 15:24:50	47.67221	8.76979	0.7	1.7	1.3	0.26	acid 2/4
2015-02-27 15:49:53	47.67548	8.76769	1.7	1.4	0.9	0.20	acid 2/4
2015-02-27 14:42:01	47.67671	8.76873	1.2	1.7	1.6	0.15	acid 2/4
2013-04-24 10:21:20	47.68161	8.76871	-0.4	1.5	1.0	0.10	mud loss
2013-05-06 15:50:01	47.68284	8.77183	-0.4	1.2	1.0	0.05	acid 1/1
2015-02-27 14:40:18	47.68161	8.77287	0.6	3.0	1.7	0.03	acid 2/4
2015-02-27 15:01:41	47.67711	8.76977	1.2	1.5	1.4	0.00	acid 2/4

The first 83 detected events occurred in close temporal correlation with massive mud losses into a fracture zone at the end of the horizontal section of the borehole in about 1'175 m TVD. Mud weights used at that time were around 1.11 – 1.15 kg/l, which indicates an overpressure above hydrostatic of 1.3 – 1.8 MPa. These small overpressures, which were sufficient to induce microseismicity up to magnitude ML0.3, indicate, that at least a subset of the fractures in the close vicinity of the borehole are nearly optimally oriented in the present stress field, and were critically stressed. With a b-value of 1.2, the earthquakes associated with the mud losses have a frequency-magnitude distribution close to the tectonic average. Both of these observations – rather small triggering overpressures and low b-value - indicate that the seismicity was caused by the reactivation of a pre-stressed fault, lubricated by the mud losses.

Most of the remaining 316 microearthquakes, were associated with the acid stimulations in SLA-2 in May 2013 and February 2015. All six individual stages of the four acid stimulations can be identified in the seismicity. The largest earthquake observed in this study, an ML0.4 event on February 25, 2015, can be associated with the second stage of the stimulation on this day (Tab. 1). First results of a more detailed analysis by Kraft et al. (2017) indicate, that the seismicity is aligned along an NNW-SSE striking lineament that extends into the formation for more than 500 m from the well in both directions. The high b-values observed for the acid stimulations hint to a fluid driven origin of the seismicity. These observations indicate, that all acid jobs mainly stimulated the same narrow lineament, but reached deep into the formation. Unfortunately, the events were too small to analyses their focal mechanisms, and it remains unknown if the lineament failed in opening or in shear mode. Yet, the high b-value of the acid-job seismicity is in the range of b-values observed in hydraulic fracturing experiments (Davies et al. 2013). This could hint at an opening-mode fracture growths along the lineament. The post-stimulation closure of the mode-I fracture could explain the limited success of the acid stimulation. Howsoever, the acid-jobs seem to have only stimulated a small narrow volume around a 2D structure, and not a larger distributed 3D volume as hoped for. This may turn out to be a limiting factor for sustainability of heat extraction from the underground at the Schlattingen site in the future.

As expected for a shallow geothermal project with small injection volumes, the seismic response of the underground to the performed operations was benign. With 0.4×10^{-3} events per day, the upper bound of the expected daily rate of potentially felt earthquakes ($ML \geq 1.7$) – extrapolated from the overall frequency-magnitude distribution of the observed - was very low. Assuming a static behavior of the induced seismicity, a felt earthquake would be statistically expected every 2500 days only. Considering that the mud-loss and acid-job seismicity, as well as the seismicity of the individual acid-jobs, had quite different b-values, the behavior of the seismicity must be classified as non-statically, at least if periods longer than on day are considered. A non-static behavior is expected for induced seismicity due to the non-static forcing of the causative geotechnical operations. Earthquake probability forecasts must, therefore, be updated in regular and small enough time intervals to be meaningful (Kiraly et al. 2017).

With the mud-loss seismicity, this study documents one of the rare cases of drilling-induced seismicity. The only other cases of drilling induced seismicity in Switzerland, that the authors are aware of, are documented in an unpublished report of the Basel geothermal project (Schanz et al. 2008), and describe a hand-full of earthquakes up to magnitude ML0.9 (Mw1.4) associated with a water-kick and a liner cementation during the drilling of the Basel-1 borehole. To our knowledge, there is no published documentation of a case of damage due to drilling induced seismicity in the scientific literature. Considering the hundreds of thousands of deep boreholes that were drilled in the last decades worldwide, the risk of experiencing a damaging drilling-induced earthquake is extremely small. Not all drilling projects are equal, and even though the hazard of drilling induced seismicity is small, the SED recommends to quantify this hazard in a short expert evaluation (Wiemer et al. 2017).

4 Acknowledgements

We thank Hansjörg Grob and Grob Gemüsebau for their permission to measure in SLA-1 and their continuous support. This project was funded by swiss energy and Nagra.

4 References

Allen, R.V. (1978): Automatic earthquake recognition and timing from single traces, Bull. Seism. Soc. Am., 68, 1521–1532.

Bläsi, H.R., Hertrich, M., Madritsch, H., Weber, H.P., & Kuhn, P. (2014): Geologie und bohrlochgeophysikalisches Logging der Geothermiebohrung Schlattingen SLA-2 (Rohdaten). Nagra Project Report NPB 13-12.

Bohnhoff, M., Dresen, G., Ellsworth, W. L., & Ito, H. (2010). Passive Seismic Monitoring of Natural and Induced Earthquakes: Case Studies, Future Directions and Socio-Economic Relevance. In S. Cloetingh & J. Negendank (Eds.), New Frontiers in Integrated Solid Earth Sciences (pp. 261–285). Springer Netherlands. http://doi.org/10.1007/978-90-481-2737-5_7

Davies, R., Foulger, G., Bindley, A., & Styles, P. (2013): Induced seismicity and hydraulic fracturing for the recovery of hydrocarbons. Marine and Petroleum Geology, 45, pp. 171 – 185.

Deichmann, N. (2017): Theoretical basis for the observed break in ML/MW scaling between small and large earthquakes. Bulletin of the Seismological Society of America, 107(2), 505 – 520.

Diehl, T., Korger, E., Clinton, J., Haslinger, F. & Wiemer, S. (2015): The Nagra weak-motion network: annual report on network performance and seismicity 2014, Technical Report, ETH Zurich.

Diehl, T., Kraft, T., Clinton, J., Haslinger, F. & Wiemer, S. (2015): The Nagra weak-motion network: annual report on network performance and seismicity 2014, Technical Report, ETH Zurich.

Egli, D., Madritsch, H., Ibele, T., Mosar, J. & Vietor, T. (2014): Stress and strain around a multiply reactivated deep-seated fault zone and its impact on a potential geothermal reservoir – The Freiburg-Bonndorf-Bodensee fault zone, Geophysical Research Abstracts, Vol. 16, (2014), EGU2014-10375, 2014 EGU General Assembly.

Frieg, B. (2015): GEOCHEM – Anwendungsorientierte Produktionsoptimierung der Geothermiebohrung Schlattingen 2. Final report to Swiss Federal Office of Energy, pp. 150, http://www.bfe.admin.ch/php/includes/container/enet/flex_enet_anzeige.php?lang=de&publication=11347&height=400&width=600.

Frieg, B., Grob, H., Hertrich, M., Madritsch, H., Müller, H., Vietor, T., Vogt, T. & Weber, H. (2015): Novel Approach for the Exploration of the Muschelkalk Aquifer in Switzerland for the CO2-free Production of Vegetables. World Geothermal Congress, Melbourne, Australia, April 19 – 25.

Gibbons, S.J. & F. Ringdal (2006): The detection of low magnitude seismic events using array-based waveform correlation, Geophys. J. Int., 165(1), 149–166.

Hermann, M., Kraft, T., Tormann, T. &Wiemer, S. (2017): One decade of induced seismicity in Basel, CH: A consistent high-resolution catalog obtained by template matching, To be submitted to the Bulletin of the Seismological Society of America.

Husen, S., Kissling, E., Deichmann, N., Wiemer, S., Giardini, D., & Baer, M. (2003): Probabilistic earthquake location in complex three-dimensional velocity models: Application to Switzerland. J. Geophys. Res., 108(B2), 2077--. Retrieved from http://dx.doi.org/10.1029/2002JB001778.

Ibele, T. (2015): Tectonics of the Hegau and Lake Constance region: A synthesis based on existing literature. Nagra Arbeitsbericht NAB 12-23.

Klee, G. (2012): Geothermal Borehole Schlattingen 1 – Hydraulic fracturing stress measurements. Nagra Project Report NPB 12-06 (unpublished).

Kraft, T., Diehl, T., Tormann, T., Herrmann, M. & Frieg, B. (2017): Induced at the Geothermel Project Schlattingen, CH. 2nd Schatzalp Workshop on Induced Seismicity, Davos, Switzerland, 14-17 March 2017, http://www.seismo.ethz.ch/export/sites/sedsite/research-and-teaching/.galleries/pdf_schatzalp/P1-09_Kraft_etal.pdf.

Király-Proag, E., V. Gischig, J.D. Zechar & S. Wiemer (2017): Multi-component ensemble models to forecast induced seismicity. Geophysical Journal International, ggx393, https://doi.org/10.1093/gji/ggx393.

Lomax, A., Virieux, J., Volant, P., & Berge, C. (2000): Probabilistic earthquake location in 3D and layered models: Introduction of a Metropolis-Gibbs method and comparison with linear locations. In C. H. Thurber & N. Rabinowitz (Eds.), Advances in Seismic Event Location (pp. 101–134). Amsterdam: Kluwer.

Madritsch, H. (2015): Outcrop-scale fracture systems in the Alpine foreland of central northern Switzerland: kinematics and tectonic context. Swiss Journal of Geosciences, 108(2–3), 155–181. http://doi.org/10.1007/s00015-015-0203-2.

Nagra (2008): Vorschlag geologischer Standortgebiete für das SMA- und das HAA-Lager – Geologische Grundlagen. Nagra Technical Report NTB 08-04.

Nagra (2000): 3D-Seismik – Räumliche Erkundung der mesozoischen Sedimentschichten im Zürcher Weinland. Nagra Technical Report NTB 00-03.

Rabinowitz, N., & Steinberg, D. M. (1990): Optimal configuration of a seismograph network: A statistical approach. Bull. Seismol. Soc. Am., 80(1), 187 – 196.

Schanz, U., Spillmann, T. & Häring, M.O. (2008): Beurteilung des Reservoirs Basel-1. Teil II. Mikroseismisches Monitoring. Final Project Report of Geothermal Explorers Ltd., pp.70, (unpublished).

Shelly, D.R., Beroza, G.C. & Ide, S. (2007): Non-volcanic tremor and low-frequency earthquake swarms, Nature, 446(7133), 305 – 307.

Sue, C., Delacou, B., Champagnac, J.-D., Allanic, C. & Burkhard, M. (2007): A seismic deformation in the Alps: GPS vs. seismic strain quantification, Terra Nova, 19(3), (2007), 182 – 188.

Vouillamoz, N., Kraft, T., Abednego, M. & Diehl, T. (2016): Lowering microseismic detection threshold in Northeastern Switzerland using sonogram analysis and template matching. Nagra Arbeitsbericht NAB 16-72 (unpublished).

Wiemer, S., Kraft, T., Trutnevyte, E. & Roth, Ph. (2017): "Good Practice" Guide for Managing induced Seismicity in Deep Geothermal Energy Projects in Switzerland. Report of the Swiss Seismological Service, Version 1.0, October 2017, http://doi.org/10.12686/a5.